

Detection of low clouds in Meteosat images based on a contextual spatio-temporal labeling approach

C. Papin*

P. Bouthemy*

G. Rochard†

*Irisa/Inria
Campus de Beaulieu
35042 Rennes Cedex, France

†Centre de Météorologie Spatiale
Avenue de Lorraine
22302 Lannion Cedex, France

Abstract

This paper presents an original method to detect low clouds at night from METEOSAT IR images. We exploit relevant motion-based measurements as well as information on the temperature and the thermal structure of the elements constituting the scene. A classification in three classes (low clouds, clear sky and other clouds) is embedded in a Bayesian estimation framework associated with Markov Random Field (MRF) models. An unsupervised learning scheme of thermal parameters associated to each class has been developed. We also propose a spatially-progressive minimization procedure of the energy function starting from reliably labelled pixels and based on the deterministic relaxation algorithm ICM. Contextual information on the label field is taken into account. Experimental results are reported and compared with ground truth. They demonstrate the efficiency of the proposed approach.

1 Introduction

Nowcasting of stratiform low clouds (SLC) as stratus and fog is very important for the security of air and road traffic. Such an identification can be achieved by exploiting the distinct emissivities of stratiform clouds in the $3.7\mu\text{m}$ and $11\mu\text{m}$ channels of the polar satellite NOAA/AVHRR. However, this can only be performed at too distant time instants. Short-time forecasting requires a higher frequency of observations provided by a geostationary satellite such as METEOSAT. Many different cloud classification methods relying on multi-spectral information were already developed. The most common approach is to classify each pixel on an individual basis. Statistical classifiers based on a dynamic clustering technique was for instance applied to METEOSAT images [4]. Cloud detection methods using threshold tests applied to different combination of channels were also considered [3]. A more specific stratus and fog detection scheme based on thresholding of the difference between $11\mu\text{m}$ and $3.7\mu\text{m}$ channels

is described in [6]. The authors reduce the number of misclassified pixels by temperature averaging and eliminating too small regions of SLC supposed physically invalid. [2] recently proposed a method combining temperature thresholding for clear sky identification, and a proximity decision rule in a 3d-feature space involving previously learned cloud parameters.

However, these pixel-wise methods tend to produce noisy results without postprocessing. Contextual labeling approaches appear to be more efficient in that sense. Such an analysis based on transition probabilities between pairs of neighboring pixels has been investigated in [7].

[10.5 – 12.5 μm] Thermal infrared (IR) is the only METEOSAT channel available during night for detecting low clouds. Then, multi-spectral analysis is not available in that case. Moreover, low clouds are often quite difficult to delineate within a single METEOSAT IR image due to the poor thermal contrast between low clouds and the earth surface. A spatio-temporal approach is therefore relevant to correctly locate such clouds.

2 Definition of observations and labels

A preliminary thresholding step allows us to separate pixels of low intensity values, i.e. cold temperatures, belonging unambiguously to medium and high clouds, from the others. Temperature thresholds are linked to the ground (or sea) temperature by a linear law, as defined in [2]. We aim at classifying the remaining pixels S into three classes consisting of low clouds, “lc”, clear sky, “cs” and other medium and high clouds “oc”. We force unambiguous high level pixels U to keep label “oc”. Depending on the amount of high level clouds within the scene, computational time can be quite reduced. We propose an original statistical contextual labeling method to solve this issue.

We have defined a two-component feature vector

involving both image intensities I and motion-based measurements ω . We can easily deduce the corresponding temperatures from intensity values I using the calibration tables provided by EUMETSAT. The motion-based observation at pixel p relies on the spatial intensity gradient ∇I , and the temporal intensity derivative I_t ; it is defined by, [8]:

$$\omega(p) = \frac{\sum_{r \in \mathcal{F}_p} (\|\nabla I(r)\| \times |I_t(r)|)}{N \times \max(G_m^2, \frac{1}{N} \sum_{r \in \mathcal{F}_p} \|\nabla I(r)\|^2)} \quad (1)$$

where \mathcal{F}_p is a window centred on p containing N pixels and G_m is a predetermined constant which can be assimilated to noise level. $\omega(p)$ can be seen as a local weighted average of the normal component (i.e. in the direction of the spatial intensity gradient) of the 2D image motion vector.

SLC are characterized by a rather smooth and featureless appearance which does not facilitate the intensity gradient-based motion evaluation. Therefore, it is important to qualify the reliability of this motion-based information at each pixel according to the spatial intensity gradient distribution in the vicinity of this pixel. Lower and upper bounds, related to observation $\omega(p)$, can be derived [8] for a given minimal low cloud displacement magnitude δ . A value of $\omega(p)$ greater than the upper bound $L(p)$ indicates that the underlying displacement magnitude is at least equal to δ . In contrast, a value of $\omega(p)$ lower than the lower bound $l(p)$ reveals a displacement lower than δ . Nothing can be straightforwardly deduced if $\omega(p)$ lies within $[l(p), L(p)]$, and then, contextual information must be exploited.

3 Statistical modelling

To formulate this labeling problem, we have adopted a statistical approach based on Bayesian estimation (MAP criterion) associated with Markov Random Field (MRF) models. The MRF framework provides a powerful formalism to specify linear and non-linear relations between observations o (temperature, motion) and the label field e (involving three classes, “lc”, “cs” and “oc”), while easily allowing to express a priori contextual information on the label field. Due to the equivalence between MRF and Gibbs distributions, [5], it turns out that this leads to the definition of a global energy function $U(o, e)$. We have designed the following energy function:

$$U(o, e) = \underbrace{\sum_{p \in \mathcal{S}} V_1(\omega(p), e(p)) + \sum_{p \in \mathcal{S}} V_2(I(p), e(p))}_{\substack{\text{data-driven term} \\ U_3(e)}} + \alpha \underbrace{\sum_{\langle p, r \rangle \in \mathcal{C}} V_3(e(p), e(r))}_{\text{regularisation term}} \quad (2)$$

where \mathcal{C} represents all the binary cliques associated with the considered second-order neighborhood system on the set of sites (pixels).

3.1 Definition of the energy terms

Potential V_2 characterizes the adequacy between the estimated label field e and the temperature map. It also takes into account a geographic mask \mathcal{G} . Thermal parameters associated to potential V_2 are the mean temperature μ_{class} and variance σ_{class}^2 where “class” stands for labels “lc” or “cs”. They are estimated for each class over different areas \mathcal{R} in the image accounting for the possible latitude-dependent variations, using an unsupervised learning scheme. To this end, each image is split into predefined homogeneous ground (or water) areas \mathcal{R} , where relevant modes are extracted either from temperature histograms of mobile pixels characterized by displacements greater than δ (in practical $\delta \in [1, 2]$) or of motionless pixels ($\omega(p) \leq l(p)$).

More information can be extracted from the analysis of thermal profile along coasts. We extract coastlines, formed by edges in the binary map \mathcal{G} , as a set of closed curves (island) or not. We compute along each curve the spatial intensity gradient in the direction normal to the curve. We assume that a small thermal variation on a large enough segment of the curve reveals the presence of stratiform clouds (see Fig. 1). These regions of low clouds are then used in the learning scheme as well as in the initialization of the minimization step.

Information on featureless SLC displacements is predominantly obtained at their boundaries. Then, we have to characterize the nature of pixels belonging to the occlusion regions. We know that, over the water, low clouds are rather colder than the water surface. There are in that case, no difficulty to determine uncovered background from moving pixels. On the other hand, low clouds located over the ground can appear warmer in case of temperature inversion within low level air. This phenomenon, referred to as “black stratus” has to be detected in order to deter-

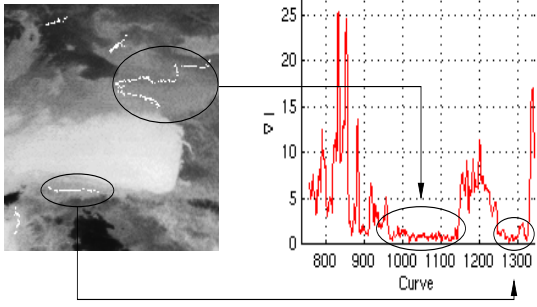


Figure 1: Example of two local detections of SLC around coastlines. In white, coastlines presenting a low spatial thermal gradient, and then supposed to be covered by low clouds.

mine the nature of the occlusion areas. Then, we build up the temperature histograms \mathcal{H}_0 of the motionless pixels with the choice of a high value of parameter G_m to get as reliable as possible information. Motionless pixels are therefore located within the most contrasted regions as coastlines or textured land ($l(p) > 0$), and not in the inner part of a SLC ($l(p) \rightarrow 0$). Extracted modes from these histograms are considered as correctly representing land temperature. These modes are compared, exploiting the Fisher distance, with those obtained from the temperature histograms of pixels verifying $\omega(p) \geq L(p)$ including invalid uncovered background pixels. Modes which are not present in \mathcal{H}_0 are then used to determine low cloud thermal parameters over land. The other ones correspond to uncovered background pixels and are eliminated.

This learning step is updated for each image along the sequence, which allows us to cope with temporal variations of the temperature modes. A robust Leclerc's estimator is used to define potential V_2 : $V_2(I(p), e(p)|g(p)) =$

$$\begin{cases} \min_{[j=1, N_{lc}]} (1 - \exp(-\frac{(I(p) - \mu_{lc}^j)^2}{(\sigma_{lc}^j)^2})) & \text{if } e(p) = lc \\ \min_{[j=1, N_{cs}]} (1 - \exp(-\frac{(I(p) - \mu_{cs}^j)^2}{(\sigma_{cs}^j)^2})) & \text{if } e(p) = cs \end{cases} \quad (3)$$

where index j indicates the j th of the N_{class} modes within a given area \mathcal{R} (Fig. 2). We handle in this way the possible presence of several characteristic temperatures within the same area for a given class. Such multi-modal situations can be caused for instance by local transparency phenomena.

Potential V_1 accounts for the intrinsic mobility and the smooth appearance of SLC with help of the confidence informations on motion-based measurements. Moreover, the use again of robust estimators [1] allows

us to deal with large deviation from the data model occurring in particular in occlusion areas.

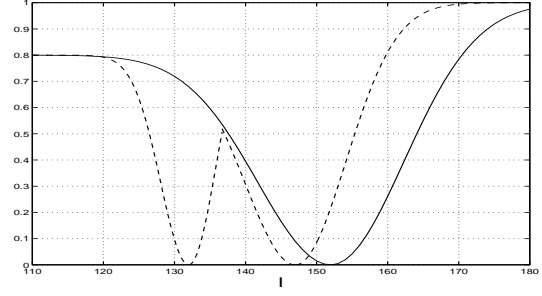


Figure 2: Thermal potential term attached to label “cs” for a given region. Two modes ($N_{cs} = 2$) have been found (dashed line) for sea area, and one mode (solid line) for ground area.

The featureless aspect of SLC results in a lack of reliable motion-based measurements verifying $\omega(p) \geq L(p)$, except in the vicinity of the cloud boundaries. In order to increase the amount of these usable motion-based measurements, we perform their calculation twice, once from t to $t + 1$ and once from $t + 1$ to t . Moreover, as explained above, we are able to determine which between low clouds or underlying ground is the warmer. Then, the test below allows us to identify the nature of an occlusion area from the sign of the temporal intensity gradient I_t :

$$\begin{cases} \omega(p) \geq L(p) & \text{and} & \text{sign}(I_t(p)) = \text{sign}(\mu_{cs} - \mu_{lc}) \\ \Rightarrow p \in \{lc, oc\} \\ \omega(p) \geq L(p) & \text{and} & \text{sign}(I_t(p)) \neq \text{sign}(\mu_{cs} - \mu_{lc}) \\ \Rightarrow p \in cs \end{cases} \quad (4)$$

where conditions expressed in (4) stands respectively for moving pixels and uncovered background. If a pixel is considered as a moving pixel, its motion-based measurement is used at time t . On the other hand, a measure $\omega(p)$ of an uncovered background pixel is stored and used at time $t + 1$.

Behaviour of potential V_1 in different situations is depicted on Fig. 3.

Case (1) corresponds to an ambiguous situation (e.g. the core of a stratiform cloud). The uncertainty interval $[l(p), L(p)]$ here tends to its maximum width $[l(p) \rightarrow 0, L(p) \rightarrow \delta]$. A low value for $\omega(p)$ thus induces a rather small difference between potentials attached to cloud labels (“lc” or “oc”) and label “cs”, since it is not discriminating by itself. In case (2), the local intensity contrast brings uncertainty bounds closer ($[l(p) \rightarrow \frac{\delta}{2}, L(p) \rightarrow \frac{\delta}{\sqrt{2}}]$), and labeling “lc” or

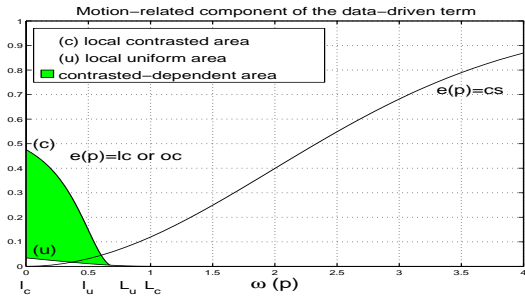


Figure 3: Motion-related component of the data-driven potential term for two configurations (uniform area (1) and contrasted area(2)) with $\delta = 1$.

“oc” is then more penalized for a motion observation lower than $L(p)$. Whatever the local intensity contrast, potential V_1 attached to labels “lc” or “oc” presents a minimum cost for $\omega(p) \geq L(p)$. Indeed, we can assume that $\omega(p) \geq L(p)$ indicates a displacement of magnitude at least equal to δ , which is usually perceptible in the vicinity of low clouds boundaries or inside textured clouds.

Potential V_3 is defined on two-site cliques $\langle p, r \rangle$, and models the spatial constraints on the label field. It is given by:

$$V_3(e(p), e(r) | \overline{\nabla I}(p)) = \begin{cases} +\beta_2 & \text{if } e(p) \neq e(r) \\ +\beta_1 \operatorname{atan}(\overline{\nabla I}(r) - \tau) & \text{if } e(p) = e(r) = lc \\ -\beta_2 & \text{if } e(p) = e(r) = cs \\ -2\beta_2 & \text{if } e(p) = e(r) = oc \end{cases} \quad (5)$$

We favour compact areas by introducing a negative potential for identically labeled neighboring sites and a positive potential otherwise. However, the smaller the local spatial image gradient magnitude, the most favoured configuration $e(p) = e(r) = lc$ since the low clouds are supposed to be rather uniform in intensity. τ determines the spatial intensity gradient magnitude from which cost becomes positive. Parameter β_2 is chosen in order to penalize configuration $e(p) = e(r) = lc$ less than configuration $e(p) \neq e(r)$ even if $\overline{\nabla I}(r)$ is high. We favour the configuration $e(p) = e(r) = oc$ over $e(p) = e(r) = lc$ in order to account for the edge of medium or high clouds. Indeed, the apparent temperature in such areas decreases and might get close to the one of low clouds.

3.2 Minimization Scheme

Our formulation of the cloud classification problem leads to the minimization of the global energy function $U(o, e)$. We have designed an iterative minimization

scheme, based on the deterministic relaxation algorithm ICM (Iterated Conditional Mode), that involves a proper handling of the initialization step, and follows a “propagative” relaxation process. The principle is to propagate information from reliable points toward areas presenting uncertain motion-based measurements. It starts in the neighborhood of most reliable pixels, called *germs* defined by:

$$\omega(p) \geq L(p) \quad \text{and} \quad \mu_{lc} - \sigma_{lc} < I(p) < \mu_{lc} + \sigma_{lc} \quad (6)$$

Moreover, pixels surrounding extracted coastlines are taken as additional germs. Label assignment of germs and neighboring sites is first realized according to a Maximum Likelihood (ML) criterion. Relaxation involving the regularisation energy term is then performed in the neighbourhood of these first labeled sites, and is progressively extended. This iterative relaxation scheme is stopped when the entire image has been processed. A step of the propagative scheme is illustrated in Fig. 4b.

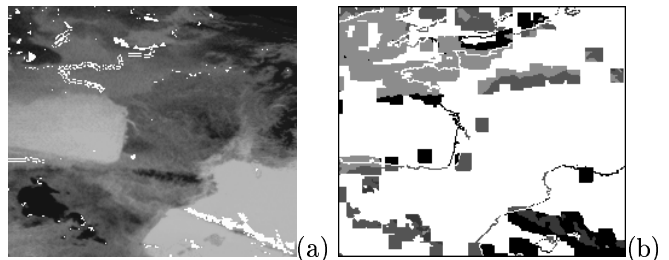


Figure 4: (a) Germs are plotted in white. (b) Second step of the “propagative” relaxation scheme. Low clouds are in light grey, clear sky in black (over sea) or grey (over land), and other clouds in dark grey. Pixels in white are not still processed.

4 Results

An example of cloud classification is provided in Fig. 5b. The processed region (Fig. 5a) is centered over Western Europe in the IR METEOSAT image acquired on October 2, 1997, at 03h30 UTC. The obtained results can be compared with a cloud classification (Fig. 5c), extracted from the polarstereographic NOAA/AVHRR image recorded at 03h27UTC, [3]. NOAA imagery permits the use of a combination of 3.7 and 11 μm IR channels, which leads to locate low clouds in an easy way. Therefore, image in (5c) can be considered as “ground truth”. We can point out that the two classifications are quite similar. In particular, one difficulty is that stratus over North of France appear warmer than ground due to a low level thermal inversion, and their temperatures differ only

from 1.5°C. Pixels presenting sufficient and reliable motion-based measurements, although rather sparse, well-contribute to correctly initialize the contextual and iterative segmentation process. Parameters β_1 , β_2 and τ are set in a heuristical way respectively to 0.1, 0.04 and 3. Similarly, G_m and δ are fixed resp. to 2 and 1.

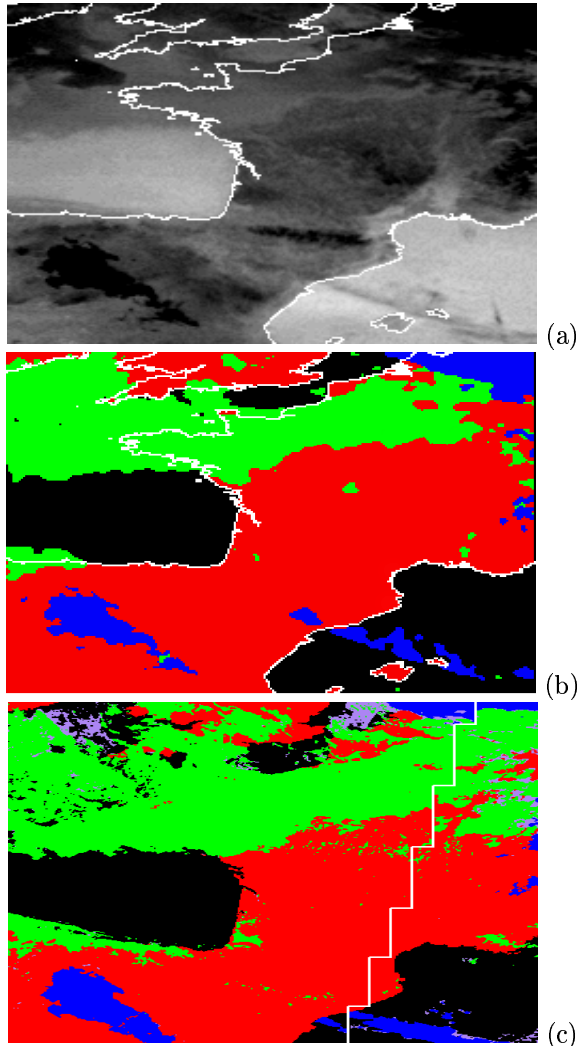


Figure 5: (a) METEOSAT enhanced IR image on October 2, 1997 at 3h30UTC. (b) Obtained classification map. Low clouds are in light grey, clear sky in black (over sea) or grey (over land), and other clouds in dark grey. (c) NOAA classification at 03h27UTC, from [3].

5 Conclusion

We have proposed an original statistical contextual labeling method to detect low clouds from IR METEOSAT images during nighttime period, which is of particular importance for every day weather

analysis and forecast, in Western Europe. The use of motion-based measurements allows us to enlarge the information supplied by the only METEOSAT IR channel available by night. Moreover, temporal coherence of the classification along the sequence is properly handled by the developed scheme. Segmentation maps can thus be animated, and can provide useful insights on the weather situation to be analysed. More results can be seen at <http://www.irisa.fr/Vista/Demos/Demos.html>.

Acknowledgments

We wish to thank the forecasters of DIR/O-Rennes for their useful advices as well as the DEMOS department of CMS-Lannion. This study is supported by Météo-France.

References

- [1] A. Blake, "On the unification of Line Processes, Outlier Rejection, and robust Statistics with Applications in Early Vision", *Int. Journal of Comp. Vision*, Vol. 19, no. 1, pp. 57-91, 1996.
- [2] A. Brisson, M. Dioszeghy, P. LeBorgne and A. Marsouin, "Classification nuageuse Météosat: expérience 1996", *Technical Report*, Météo-France/SCM/CMS, Lannion, 1997.
- [3] M. Derrien, B. Farki, L. Harang, H. Le Gleau, A. Noyalet, D. Pochic and A. Sairouni, "Automatic Cloud Detection Applied to NOAA-11/AVHRR Imagery", *Remote Sensing of Environment*, Vol. 46, no. 3, pp. 246-267, 1993.
- [4] M. Desbois, G. Sèze and G. Szejwach, "Automatic classification of clouds on Meteosat imagery: application to high level clouds", *J. Appl. Meteorol*, Vol. 21, pp. 401-412, 1982.
- [5] S. Geman and D. Geman, "Stochastic relaxation, Gibbs distributions and the Bayesian restoration of images", *IEEE Trans. on Pattern Anal. and Machine Intel.*, Vol. 6, no. 6, pp. 721-741, 1984.
- [6] J.P. Nelson and G.P. Ellrod, "Improved GOES-8 multispectral satellite imagery to detect stratus and fog at night", *8th Conf. on Sat. Meteorol. and Oceano.*, AMS, Atlanta, pp. 172-175, 1996.
- [7] J. Kittler and D. Pairman, "Contextual pattern recognition applied to cloud detection and identification", *IEEE Trans. on Geoscience and Remote Sensing*, Vol. 23., pp. 855-863, 1985.
- [8] J-M. Odobez and P. Bouthemy, "Separation of moving regions from background in an image sequence acquired with a mobile camera", H.H. Li and S. Sun and H. Derin editors, *Video Data Compression for Multimedia Computing*, Kluwer Academic Publisher, Chap. 7, pp. 283-311, 1997.